Plasmon-induced transparency in a single multimode stub resonator

Guangtao Cao,[1, 2, 3] Hongjian Li,[1, 2,*] Yan Deng,[3] Shiping Zhan,[1] Zhihui He,[1] and Boxun Li[1]

[1]*College of Physics and Electronics, Central South University, Changsha 410083, China*
[2]*College of Materials Science and Engineering, Central South University, Changsha 410083, China*
[3]*College of Physics, Mechanical and Electrical Engineering, Jishou University, Jishou 416000, China*
[*] *lihj398@126.com*

Abstract: We investigate electromagnetically induced transparency (EIT)-like effect in a metal–dielectric–metal (MDM) waveguide coupled to a single multimode stub resonator. Adjusting the geometrical parameters of the stub resonator, we can realize single or double plasmon-induced transparency (PIT) windows in the plasmonic structure. Moreover, the consistency between analytical results and finite difference time domain (FDTD) simulations reveals that the PIT results from the destructive interference between resonance modes in the stub resonator. Compared with previous EIT-like scheme based on MDM waveguide, the plasmonic system takes the advantages of easy fabrication and compactness. The results may open up avenues for the control of light in highly integrated optical circuits.

OCIS codes: (240.6680) Surface plasmons; (230.7370) Waveguides; (130.3120) Integrated optics devices.

References and links

1. K. J. Boller, A. Imamolu, and S. E. Harris, "Observation of electromagnetically induced transparency," Phys. Rev. Lett. **66**(20), 2593–2596 (1991).
2. M. Fleischhauer, A. Imamoglu, and J. P. Marangos, "Electromagnetically induced transparency: optics in coherent media," Rev. Mod. Phys. **77**(2), 633–673 (2005).
3. I. Novikova, R. L. Walsworth, and Y. Xiao, "Electromagnetically induced transparency-based slow and stored light in warm atoms," Laser Photon. Rev. **6**(3), 333–353 (2012).
4. J. J. Chen, Z. Li, S. Yue, J. H. Xiao, and Q. H. Gong, "Plasmon-induced transparency in asymmetric T-shape single slit," Nano Lett. **12**(5), 2494–2498 (2012).
5. Z. R. Zhang, L. W. Zhang, H. Q. Li, and H. Chen, "Plasmon induced transparency in a surface plasmon polariton waveguide with a comb line slot and rectangle cavity," Appl. Phys. Lett. **104**(23), 231114 (2014).
6. X. Y. Yang, X. Y. Hu, Z. Chai, C. C. Lu, H. Yang, and Q. H. Gong, "Tunable ultracompact chip-integrated multichannel filter based on plasmon-induced transparencies," Appl. Phys. Lett. **104**(22), 221114 (2014).
7. Y. Huang, C. Min, and G. Veronis, "Subwavelength slow-light waveguides based on a plasmonic analogue of electromagnetically induced transparency," Appl. Phys. Lett. **99**(14), 143117 (2011).
8. H. Lu, X. M. Liu, and D. Mao, "Plasmonic analog of electromagnetically induced transparency in multi-nanoresonator-coupled waveguide systems," Phys. Rev. A **85**(5), 053803 (2012).
9. L. Chen, C. M. Gao, J. M. Xu, X. F. Zang, B. Cai, and Y. M. Zhu, "Observation of electromagnetically induced transparency-like transmission in terahertz asymmetric waveguide-cavities systems," Opt. Lett. **38**(9), 1379–1381 (2013).
10. Y. Zhu, X. Y. Hu, H. Yang, and Q. H. Gong, "Ultralow-power all-optical tunable double plasmon-induced transparencies in nonlinear metamaterials," Appl. Phys. Lett. **104**(21), 211108 (2014).
11. Z. H. Han and S. I. Bozhevolnyi, "Plasmon-induced transparency with detuned ultracompact Fabry-Perot resonators in integrated plasmonic devices," Opt. Express **19**(4), 3251–3257 (2011).
12. Z. H. Han, C. E. Garcia-Ortiz, I. P. Radko, and S. I. Bozhevolnyi, "Detuned-resonator induced transparency in dielectric-loaded plasmonic waveguides," Opt. Lett. **38**(6), 875–877 (2013).
13. Y. Zhu, X. Y. Hu, H. Yang, and Q. H. Gong, "On-chip plasmon-induced transparency based on plasmonic coupled nanocavities," Sci Rep **4**, 3752 (2014).
14. G. T. Cao, H. J. Li, S. P. Zhan, H. Q. Xu, Z. M. Liu, Z. H. He, and Y. Wang, "Formation and evolution mechanisms of plasmon-induced transparency in MDM waveguide with two stub resonators," Opt. Express **21**(8), 9198–9205 (2013).
15. R. Hokari, Y. Kanamori, and K. Hane, "Comparison of electromagnetically induced transparency between silver, gold, and aluminum metamaterials at visible wavelengths," Opt. Express **22**(3), 3526–3537 (2014).

#217583 - $15.00 USD Received 22 Jul 2014; revised 17 Sep 2014; accepted 29 Sep 2014; published 8 Oct 2014

16. X. Y. Zhou, L. Zhang, W. Pang, H. Zhang, Q. R. Yang, and D. H. Zhang, "Phase characteristics of an electromagnetically induced transparency analogue in coupled resonant systems," New J. Phys. **15**(10), 103033 (2013).
17. Z. Zou, L. J. Zhou, X. M. Sun, J. Y. Xie, H. K. Zhu, L. J. Lu, X. W. Li, and J. P. Chen, "Tunable two-stage self-coupled optical waveguide resonators," Opt. Lett. **38**(8), 1215–1217 (2013).
18. W. Tan, Y. Sun, Z. G. Wang, and H. Chen, "Manipulating electromagnetic responses of metal wires at the deep subwavelength scale via both near-and far-field couplings," Appl. Phys. Lett. **104**(9), 091107 (2014).
19. M. Miyata, J. Hirohata, Y. Nagasaki, and J. Takahara, "Multi-spectral plasmon induced transparency via in-plane dipole and dual-quadrupole coupling," Opt. Express **22**(10), 11399–11406 (2014).
20. G. T. Cao, H. J. Li, S. P. Zhan, Z. H. He, Z. B. Guo, X. K. Xu, and H. Yang, "Uniform theoretical description of Plasmon-induced transparency in plasmonic stub waveguide," Opt. Lett. **39**(2), 216–219 (2014).
21. X. J. Piao, S. Yu, and N. Park, "Control of Fano asymmetry in plasmon induced transparency and its application to plasmonic waveguide modulator," Opt. Express **20**(17), 18994–18999 (2012).
22. H. Lu, X. M. Liu, D. Mao, Y. K. Gong, and G. X. Wang, "Induced transparency in nanoscale plasmonic resonator systems," Opt. Lett. **36**(16), 3233–3235 (2011).
23. V. Intaraprasonk and S. H. Fan, "Enhancing the waveguide-resonator optical force with an all-optical on-chip analog of electromagnetically induced transparency," Phys. Rev. A **86**(6), 063833 (2012).
24. J. T. Liu, B. Z. Xu, H. F. Hu, J. Zhang, X. Wei, Y. Xu, and G. F. Song, "Tunable coupling-induced transparency band due to coupled localized electric resonance and quasiguided photonic mode in hybrid plasmonic system," Opt. Express **21**(11), 13386–13393 (2013).
25. S. I. Bozhevolnyi, *Plasmonic Nanoguides and Circuits* (Pan Stanford Publishing Pte. Ltd., 2009).
26. Z. H. Han and S. I. Bozhevolnyi, "Radiation guiding with surface plasmon polaritons," Rep. Prog. Phys. **76**(1), 016402 (2013).
27. W. S. Cai, W. Shin, S. H. Fan, and M. L. Brongersma, "Elements for plasmonic nanocircuits with three-dimensional slot waveguides," Adv. Mater. **22**(45), 5120–5124 (2010).
28. I. Zand, M. S. Abrishamian, and P. Berini, "Highly tunable nanoscale metal-insulator-metal split ring core ring resonators (SRCRRs)," Opt. Express **21**(1), 79–86 (2013).
29. A. Akjouj, G. Leveque, S. Szunerits, Y. Pennec, B. Djafari-Rouhani, R. Boukherroub, and L. Dobrzynski, "Nanometal Plasmon polaritons," Surf. Sci. Rep. **68**(1), 1–67 (2013).
30. J. W. Qi, Z. Q. Chen, J. Chen, Y. D. Li, W. Qiang, J. J. Xu, and Q. Sun, "Independently tunable double Fano resonances in asymmetric MIM waveguide structure," Opt. Express **22**(12), 14688–14695 (2014).
31. T. S. Wu, Y. M. Liu, Z. Y. Yu, Y. W. Peng, C. G. Shu, and H. Ye, "The sensing characteristics of plasmonic waveguide with a ring resonator," Opt. Express **22**(7), 7669–7677 (2014).
32. J. J. Chen, C. W. Sun, and Q. H. Gong, "Fano resonances in a single defect nanocavity coupled with a plasmonic waveguide," Opt. Lett. **39**(1), 52–55 (2014).
33. Z. Chai, X. Y. Hu, Y. Zhu, S. B. Sun, H. Yang, and Q. H. Gong, "Ultracompact chip-integrated electromagnetically induced transparency in a single plasmonic composite nanocavity," Adv. Optical Mater. **2**(4), 320–325 (2014).
34. K. H. Wen, L. S. Yan, W. Pan, B. Luo, Z. Guo, Y. H. Guo, and X. G. Luo, "Electromagnetically induced transparency-like transmission in a compact side-coupled T-shaped resonator," J. Lightwave Technol. **32**(9), 1701–1707 (2014).
35. Q. Z. Huang, Z. Shu, G. Song, J. G. Chen, J. S. Xia, and J. Z. Yu, "Electromagnetically induced transparency-like effect in a two-bus waveguides coupled microdisk resonator," Opt. Express **22**(3), 3219–3227 (2014).
36. Y. F. Xiao, L. He, J. Zhu, and L. Yang, "Electromagnetically induced transparency-like effect in a single polydimethylsiloxane coated silica microtoroid," Appl. Phys. Lett. **94**(23), 231115 (2009).
37. B. B. Li, Y. F. Xiao, C. L. Zou, Y. C. Liu, X. F. Jiang, Y. L. Chen, Y. Li, and Q. H. Gong, "Experimental observation of Fano resonance in a single whispering-gallery microresonator," Appl. Phys. Lett. **98**(2), 021116 (2011).
38. Y. Matsuzaki, T. Okamoto, M. Haraguchi, M. Fukui, and M. Nakagaki, "Characteristics of gap plasmon waveguide with stub structures," Opt. Express **16**(21), 16314–16325 (2008).
39. X. S. Lin and X. G. Huang, "Tooth-shaped plasmonic waveguide filters with nanometeric sizes," Opt. Lett. **33**(23), 2874–2876 (2008).
40. E. D. Palik, *Handbook of Optical Constants in Solids* (Academic, 1982).
41. C. W. Gardiner and P. Zoller, *Quantum Noise*, 3rd ed. (Springer, Berlin, 2004).
42. Y. R. He, H. Zhou, Y. Jin, and S. L. He, "Plasmon induced transparency in a dielectric waveguide," Appl. Phys. Lett. **99**(4), 043113 (2011).

1. Introduction

Electromagnetically induced transparency (EIT) realized in atomic media originates from the quantum destructive inference between the excitation pathways to atomic upper level [1–3]. The EIT effect has potential applications for optical data storage and biosensor. However, the strict restrictions on the realization of the EIT hinder its practical application, which encourages an ongoing search for mimicking EIT in classical systems [4–24]. Surface plasmon polaritons (SPPs) trapped on the metal-dielectric interface can break the classical diffraction limit and manipulate light in the nanoscale domain [25–32]. Among various

#217583 - $15.00 USD Received 22 Jul 2014; revised 17 Sep 2014; accepted 29 Sep 2014; published 8 Oct 2014

plasmonic guiding structures, MDM waveguides, which are easily fabricated and have deep subwavelength confinement of light with an acceptable propagation length for SPPs, have attracted much attention [5, 8, 14, 20, 21, 28, 32].

Based on the unique feature of MDM waveguide, the analog of EIT observed in the coupled optical resonator systems was theoretically predicted and experimentally demonstrated in recent research [5–9, 11, 13, 14, 20–23]. Zhang and associates introduced the EIT-like phenomena inside a plasmonic waveguide configuration with a comb line slot and rectangle cavity at infrared frequencies [5]. Han et al. demonstrated the PIT using detuned Fabry-Perot resonators aperture-side-coupled to a MDM waveguide [11]. A uniform theoretical model, for both direct and indirect couplings between the two stubs, was established to study PIT in the plasmonic stub waveguide [20], and Gong et al. realized on-chip PIT in a plasmonic waveguide side-coupled to a nanocavity pair [13]. Recently, without employment of additional optical elements, EIT-like phenomena were demonstrated in a single plasmonic composite nanocavity [33, 34] or whispering-gallery microresonator [35–37]. However, there have been few studies on EIT-like in plasmonic MDM waveguide platform using a single stub resonator.

In this work, we numerically and analytically investigate the PIT spectral response in a plasmonic system composed of a MDM bus waveguide coupled to a single multimode stub resonator. The stub structure based on MDM waveguide was first reported by Matsuzaki et al. [38]. It is well known that the stub has the advantages of small size and simple structure. Therefore, various components based on the stub structure have been demonstrated [7, 9, 13, 14, 20, 21]. Here, the configuration is also based on a single stub, but it exhibits different transmission characteristics as compared with [39]. In particular, the proposed system is more easily fabricated than previously reported PIT structures [5–9, 11, 13, 14, 20–23, 33, 34], and we can observe single or double PIT windows in the plasmonic waveguide system. Therefore, this work may pave the way for the realization of nanoscale optical devices.

2. Analytical model

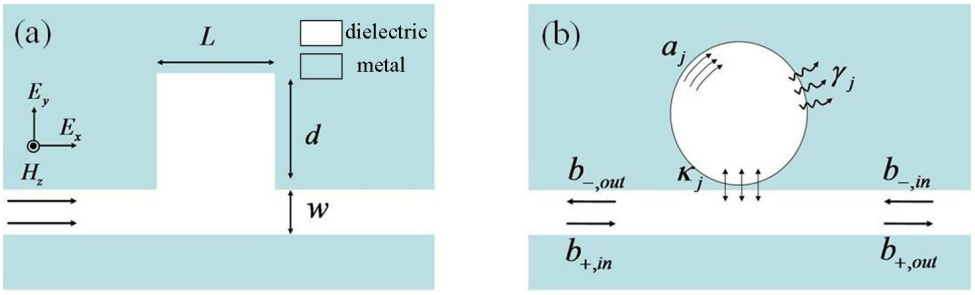

Fig. 1. (a) Schematic of MDM waveguide coupled to a stub resonator. (b) Equivalent theoretical model for Fig. 1(a).

Figure 1(a) schematically shows MDM bus waveguide side-coupled to a stub resonator. The dielectric and metal in the structure are air and silver, respectively. The permittivity of silver is described by Drude model $\varepsilon(\omega) = 1 - \omega_p^2/(\omega^2 + i\omega\gamma_p)$, with $\omega_p = 1.38 \times 10^{16}$ rad/s and $\gamma_p = 2.73 \times 10^{13}$ rad/s. These parameters are obtained by fitting the experimental results [40]. ω is the angular frequency of incident light. The main structure parameters are the width (w) of bus waveguide, length (d) and width (L) of the stub resonator. As the TM polarization light is incident along x-axis, SPP wave can be formed on metal-insulator interface and confined in the waveguide. The width L of the stub resonator is large enough that the plasmonic stub resonator can provide multiple cavity modes. Using the quantum optics, we study a waveguide-coupled multimode system, as illustrated in Fig. 0.1(b). The Hamiltonian of the system can be written as [36, 37, 41]

#217583 - $15.00 USD Received 22 Jul 2014; revised 17 Sep 2014; accepted 29 Sep 2014; published 8 Oct 2014

$$H=\sum_{j=1}^{N}\omega_j a_j^{+}a_j+\sum_{p=\pm}\int_{-\infty}^{+\infty}d\omega\omega b_p^{+}(\omega)b_p(\omega)+i\sum_{j=1}^{N}\sum_{p=\pm}\int_{-\infty}^{+\infty}d\omega\kappa_j(\omega)[b_p^{+}(\omega)a_j-a_j^{+}b_p(\omega)], \quad (1)$$

where the first two terms are the free Hamiltonian of the cavity and waveguide modes, respectively, and the last term describes the coupling between the waveguide mode and cavity modes. a_j (a^{+}_j) denotes the annihilation (creation) operator related to cavity mode j with resonance frequency ω_j. b_p (b^{+}_p) is the annihilation (creation) operator for the waveguide mode and the subscript ($p = \pm$) represents two propagating directions of waveguide mode, which satisfies the commutation relation $[b_p(\omega), b^{+}_p(\omega')] = \delta(\omega-\omega')$. The coupling coefficient κ_j describes the coupling between cavity mode j and waveguide mode.

The Heisenberg equations of motion for the waveguide and cavity modes can be given by

$$\frac{db_p(\omega)}{dt}=-i\omega b_p(\omega)+\sum_{j=1}^{N}\kappa_j(\omega)a_j, \quad (2)$$

$$\frac{da_j}{dt}=-i\omega_j a_j-\frac{\gamma_j}{2}a_j-\sum_{p=\pm}\int_{-\infty}^{+\infty}d\omega\kappa_j(\omega)b_p(\omega), \quad (3)$$

where γ_j is the intrinsic-loss rate of the jth cavity mode. By solving Eq. (2), we obtain

$$b_p(\omega)=e^{-i\omega(t-t_0)}b_{p,0}(\omega)+\sum_{j'=1}^{N}\kappa_{j'}(\omega)\int_{t_0}^{t}e^{-i\omega(t-t')}a_{j'}(t')dt'. \quad (4)$$

Here $b_{p,0}(\omega)$ is the value of $b_p(\omega)$ at $t = t_0$. Substituting Eq. (4) into Eq. (3), we get

$$\begin{aligned}\frac{da_j}{dt}&=-i\omega_j a_j-\frac{\gamma_j}{2}a_j\\&-\sum_{p=\pm}\int_{-\infty}^{+\infty}d\omega\kappa_j(\omega)\left\{e^{-i\omega(t-t_0)}b_{p,0}(\omega)+\sum_{j'=1}^{N}\kappa_{j'}(\omega)\int_{t_0}^{t}e^{-i\omega(t-t')}a_{j'}(t')dt'\right\}.\end{aligned} \quad (5)$$

Applying $\int_{-\infty}^{+\infty}d\omega e^{-i\omega(t-t')}=2\pi\delta(t-t')$, $\int_{t_0}^{t}a_j(t')\delta(t-t')=a_j(t)/2$ and the first Markov approximation $\kappa_j(\omega)=(\kappa_j/2\pi)^{1/2}$, Eq. (5) can be simplified into

$$\frac{da_j}{dt}=-i\omega_j a_j-\frac{\gamma_j}{2}a_j-\kappa_j a_j-\sum_{j'=1,j'\neq j}^{N}\sqrt{\kappa_j\kappa_{j'}}a_{j'}-\sum_{p=\pm}\sqrt{\kappa_j}b_{p,in}(t), \quad (6)$$

in which the input field $b_{p,in}(t)=\frac{1}{\sqrt{2\pi}}\int_{-\infty}^{+\infty}e^{-i\omega(t-t_0)}b_{p,0}(\omega)$. With the conservation of energy in microcavity system [20–22, 36, 37], we have

$$b_{p,out}(t)=b_{p,in}(t)+\sum_{j=1}^{N}\sqrt{\kappa_j}a_j, \quad (7)$$

where $\kappa_j^{1/2}a_j$ stands for the fields coupled out from cavity mode j. If the incident light is injected only from the left port ($b_{-,in} = 0$), the transmission coefficient through the system is $t = b_{+,out} / b_{+,in}$. The transmittance efficiency can be derived as $T = |t|^2$. Using the theoretical analysis mentioned above, we can analyze the spectra responses in the plasmonic system composing of multimode stub resonator side-coupled to MDM waveguide.

#217583 - $15.00 USD Received 22 Jul 2014; revised 17 Sep 2014; accepted 29 Sep 2014; published 8 Oct 2014

3. Simulation results and discussions

Figure 2(a) shows the transmission spectra from the same constructive parameters (w = 100nm, L = 300m), yet with d = 300nm, 340nm, 380nm, 400nm. It is obvious that a transparent window grows in strength and becomes more prominent as d increases from 300nm to 400nm. For the lossless metal case, the transmission spectra for d = 380nm (black dashed line) is also shown in Fig. 2(a). It can be seen that the transparent bandwidth keeps unchanged and we can obtain unity peak transmission in the transparent window.

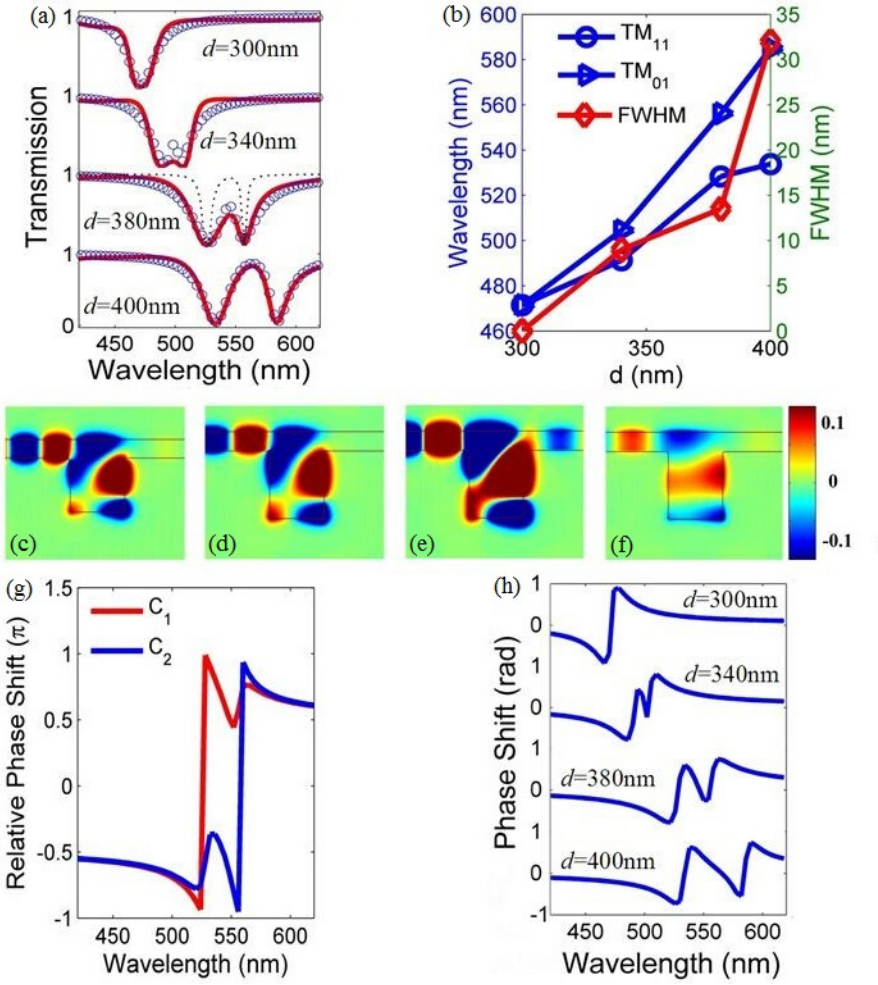

Fig. 2. (a) Transmission spectra versus different d. The solid curves are the simulation results and the circles are theoretical fittings. The black dashed line is the transmission spectra for lossless metal case (d = 380nm). The other geometrical parameters are w = 100nm, L = 300nm. (b) The resonant wavelengths of TM_{11} and TM_{02} modes, and the FWHM of transparent window versus d. Field distributions (H_z) of SPPs in the plasmonic system for d = 300nm at wavelength (c) λ = 471.5nm. For d = 380nm, field distributions (H_z) of SPPs at different wavelengths (d) λ = 528.3nm, (e) λ = 545.8nm, and (f) λ = 556.2nm. (g) The phases of coupling-out field corresponding to TM_{11} (red line) and TM_{02} (blue line) modes for d = 380nm in Fig. 2(a). (h) The transmission phase shift corresponding to Fig. 2(a). The fitting parameters are set as (d = 300nm) [λ_1, λ_2] = [471.5, 471.5] nm, [κ_1, κ_2, γ_1, γ_2] = [4.995, 4.995, 2.497, 2.497] 10^{13}rad/s; (d = 340nm) [λ_1, λ_2] = [491.3, 504.5] nm, [κ_1, κ_2, γ_1, γ_2] = [7.67, 3.73, 4.26, 2.5] 10^{13}rad/s; (d = 380nm) [λ_1, λ_2] = [528.3, 556.2] nm, [κ_1, κ_2, γ_1, γ_2] = [8.92, 4.84, 4.46, 3.76] 10^{13}rad/s; (d = 400nm) [λ_1, λ_2] = [533.8, 585] nm, [κ_1, κ_2, γ_1, γ_2] = [7.06, 4.03, 3.92, 2.48] 10^{13}rad/s.

#217583 - $15.00 USD Received 22 Jul 2014; revised 17 Sep 2014; accepted 29 Sep 2014; published 8 Oct 2014

The contour profiles of field H_z at different wavelengths are depicted in Figs. 2(c-f). Figure 2(c) corresponds to the resonant wavelength λ = 471.5nm for d = 300nm. Figures 2(d-f) illustrate z-component magnetic field, for the case of d = 380nm, at wavelengths λ = 528.3nm, 545.8nm, 556.2nm, respectively. The results in Figs. 2(c-f) are in conformity with the transmission spectra in Fig. 2(a). For the plasmonic stub structure, the resonance modes are denoted by TM_{mn}, where m and n denote the number of node of standing waves in horizontal and vertical directions in the stub resonator. Using the definition of resonance mode, we aim to investigate the evolution of transmission spectra versus d. Figure 2(b) shows the resonant wavelengths and full width at half maximum (FWHM) of the transparent window in Fig. 2(a). Combining Fig. 2(a) and Fig. 2(b), we observe that both the wavelengths of resonance modes present red shift and the transparency window progressively widens with the increase of d.

As illustrated in Fig. 2(a), two resonance modes are simultaneously excited in the plasmonic stub system. In other words, the increase of d lifts the degeneracy of TM_{11} and TM_{02} modes. Based on the FDTD, we numerically extract the related physical parameters and obtain the theoretical results denoted by circles. It can be seen that the theoretical results, for the case of N = 2, are in good agreement with the FDTD simulations, which validates the correctness of the analytical model. So, the theoretical analysis allows us to understand the response of the plasmonic resonance system explicitly. From Eq. (7), we can see that the performance of the plasmonic system is dependent on the phase shift of coupling-out field $\kappa_j^{1/2}a_j$ denoted by C_j. Consequently, to get insight into the physics of the EIT-like phenomena, we study, for d = 380nm in Fig. 2(g), the phase shifts of C_1 and C_2 corresponding to TM_{11} and TM_{02} mode, respectively. According to Eq. (6), we obtain that phase shifts of C_1 and C_2 are related to the input signal $b_{+,in}$. Moreover, the interaction between C_1 and C_2 is determined by the relative phase shift of the two coupling-out fields and the phase difference between C_1 and C_2 is independent of the input signal $b_{+,in}$. As shown in Fig. 2(g), the coupling-out field C_1 nearly has a $\sim\pi$ phase difference with C_2, which leads to the transparent response [35]. Therefore, the EIT-like optical response results from destructive interference between TM_{11} and TM_{02} modes through the MDM bus waveguide, which is similar to the formation mechanisms of PIT in previously reported coupled-resonator structures [6, 8, 11, 14, 20].

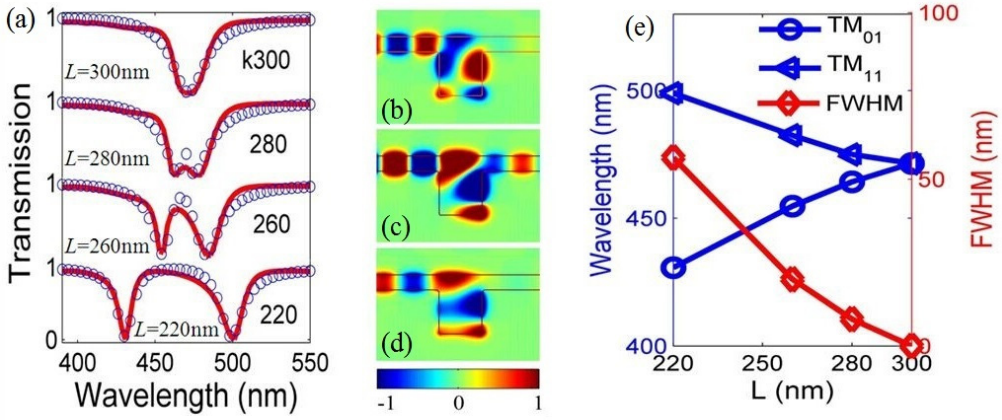

Fig. 3. (a) Transmission spectra as a function of L. The solid lines are the simulation results and the circles are the analytical model results. The other geometrical parameters are w = 100nm, d = 300nm. Field distributions (H_z) of SPPs in the plasmonic system for L = 260nm at different wavelengths (b) λ = 454.8nm, (c) λ = 463.3nm, and (d) λ = 482.6nm. (e) The resonant wavelengths and FWHM of transparent window versus L. The fitting parameters are set as (L = 300nm) $[\lambda_1, \lambda_2]$ = [471.5, 471.5] nm, $[\kappa_1, \kappa_2, \gamma_1, \gamma_2]$ = [4.995, 4.995, 2.497, 2.497] 10^{13}rad/s; (L = 280nm) $[\lambda_1, \lambda_2]$ = [464.3, 475] nm, $[\kappa_1, \kappa_2, \gamma_1, \gamma_2]$ = [5.07, 6.61, 2.54, 3.31] 10^{13}rad/s; (L = 260nm) $[\lambda_1, \lambda_2]$ = [454.8, 482.6] nm, $[\kappa_1, \kappa_2, \gamma_1, \gamma_2]$ = [5.18, 6.51, 2.59, 3.26] 10^{13}rad/s; (L = 220nm) $[\lambda_1, \lambda_2]$ = [430.7, 499] nm, $[\kappa_1, \kappa_2, \gamma_1, \gamma_2]$ = [5.15, 5.39, 2.57, 2.7] 10^{13}rad/s.

#217583 - $15.00 USD Received 22 Jul 2014; revised 17 Sep 2014; accepted 29 Sep 2014; published 8 Oct 2014

Slow light is one of the most important applications for EIT effect in atom systems, and the plasmonic system also supports slow group velocities [8, 20, 34]. $\tau_g = d\theta/d\omega$ and $\theta = arg(t)$ denote the optical delay time and transmission phase shift, respectively. The dispersion of transmission phase shift versus λ is plotted in Fig. 2(h). The normal dispersion, which leads to a significantly enhanced group delay, occurs in the transparent window, and the abnormal dispersion, which results in the negative group delay corresponding to the fast light (not discussed here), occurs around the plasmonic resonance modes. Combining Fig. 2(a) and Fig. 2(h), we can conclude that there is a trade-off between transmission ratio and the optical delay time, which agrees well with [7, 8, 20]. The EIT-like spectral response obtained by adjusting the length of the stub resonator may play an important role for the dynamic control of light in nanostructures. What impact does the width of stub resonator have on PIT effect?

In Fig. 3(a), we plot the transmission spectra as d = 300nm, w = 100nm, and L = 300, 280, 260, 220nm, respectively. Obviously, the FDTD simulations are in excellent agreement with the theoretical fittings. The transmission spectra exhibit typical EIT-like line shape with the decrease of L, and the transparency peak exhibits asymmetry, which is dependent on the coupling parameter κ_j and intrinsic-loss rate γ_j. The field distributions at mode TM_{11}, transparency-resonance wavelength and mode TM_{02} are, respectively, depicted in Figs. 3(b-d). Both Figs. 3(b) and 3(d) show that the incident light is reflected as the local resonance is excited. In Fig. 3(c), the input light at the transparency-resonance wavelength can pass through the waveguide, which also originates from the destructive interference between modes TM_{11} and TM_{02}. The resonant wavelengths of all modes versus L are plotted in Fig. 3(e). It is seen that TM_{11} mode presents red shift with the decrease of L, whereas the TM_{02} mode exhibits blue shift. The FWHM of the transparent window is also plotted in Fig. 3(e). Comparing Fig. 2(b) with Fig. 3(e), we find that the FWHM of transparent window to the width L of stub resonator is more sensitive than to the length of it, which offers a convenient scheme to control the bandwidth of transparent window. When L is larger than 300nm, whether the transmission spectra are similar to those in Fig. 3(a)?

Figure 4(a) illustrates the transmission spectra versus L. As shown in Fig. 4(a), the plasmonic system exhibits double EIT-like peaks when adjusting L from 360nm to 440nm. We note that the double EIT-like spectral response was only achieved in three-resonator system [8], highlighting our idea for the realization of double PIT windows in a single stub resonator. Figures 4(c-g) show z-component magnetic field, for the case of L = 420nm, at λ = 461.6nm, 482.9nm, 491.9nm, 498nm and 504.3nm, respectively. Figures 4(c), 4(e) and 4(g) show the profiles of field H_z of transmission dips corresponding to TM_{11}, TM_{02} and TM_{20} modes, respectively. The resonant wavelengths of all modes versus L are plotted in Fig. 4(b). The resonant wavelength for TM_{11} (TM_{02}) mode is in the range of 461.5-463.3nm (481.3-491.6nm), that is to say, they are nearly constant for L in the range of 360-440nm. However, in contrast to them, TM_{20} mode responds linearly to L. The fact indicates that the resonant modes are related to different formation and evolution mechanisms, and therefore it facilitates the dual-spectral PIT effects.

The transmission spectra calculated by the theoretical model is in good accordance with the FDTD method, from which the theoretical analysis also allows us to understand the dual-peak EIT-like response of the plasmonic resonator system. Consequently, in Fig. 4(h), we plot the phase shifts of coupling-out fields C_1, C_2 and C_3 (corresponding to TM_{11}, TM_{02} and TM_{20}, respectively), for L = 420nm in Fig. 4(a), to analyze the dual-peak EIT-like response. In the left transparent window, C_2 and C_3 are in phase, but the coupling-out field C_1 nearly has a $\sim\pi$ phase difference with $C_2 + C_3$, which leads to the transparent response. The other transparent peak, shown in Fig. 4(h), is attributed to the destructive interference between C_3 and $C_1 + C_2$. The optical responses, for the cases of L = 360nm, 380nm, 400nm, and 440nm, can also be understood by studying the phase shifts of the coupling-out field. The dispersions of transmission phase shift are represented in Fig. 4(i), which indicates that normal dispersion occurs in the transparent windows. From the analytical model, the optical delay time in the transparent window is affected by the intrinsic loss in the stub resonator, which is consistent with [11, 42]. The transmission efficiency in the transparent window is associated with the

#217583 - $15.00 USD Received 22 Jul 2014; revised 17 Sep 2014; accepted 29 Sep 2014; published 8 Oct 2014

phase shift of the coupling-out field, and is also affected by the intrinsic loss in the resonator. Thus, the incorporation of gain media in the plasmonic waveguide system compensates the intrinsic loss and enhances the EIT-like effect [42]. As mentioned above, the single multimode stub scheme, which is more compact and easily fabricated than coupled resonator systems [5–9, 11, 13, 14, 20–23], may provide a possible way to realize the required EIT-like phenomena.

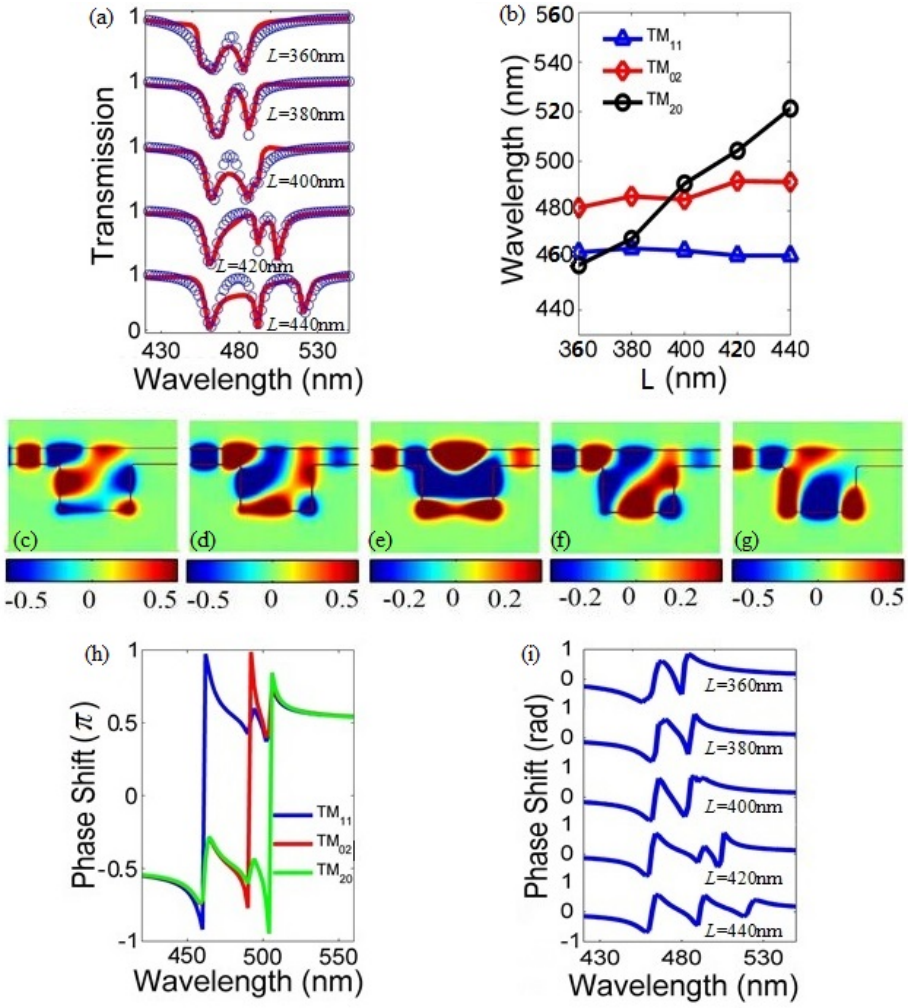

Fig. 4. (a) Simulation (solid curve) and theoretical (circles) transmission spectra with different L in the plasmonic stub waveguide. The other geometrical parameters are w = 100nm, d = 300nm. (b) The resonant wavelengths of TM_{11}, TM_{02} and TM_{20} modes versus L. Field distributions (H_z) of SPPs in the plasmonic system for L = 420nm at different wavelengths (c) λ = 461.6nm, (d) λ = 482.9nm, (e) λ = 491.9nm, (f) λ = 498nm, and (g) λ = 504.3nm. (h) The phases of TM_{11} (blue line), TM_{02} (red line) and TM_{20} (green line) modes for L = 420nm in Fig. 4(a). (i) The transmission phase shift with different L in the plasmonic structure plotted in Fig. 1(a). The fitting parameters are set as (L = 360nm) [λ_1, λ_2, λ_3] = [463.3, 481.3, 458.2] nm, [κ_1, κ_2, κ_3, γ_1, γ_2, γ_3] = [7.4, 3.26, 0.457, 4.07, 1.63, 2.06] 10^{13}rad/s; (L = 380nm) [λ_1, λ_2, λ_3] = [464.9, 485.9, 468.7] nm, [κ_1, κ_2, κ_3, γ_1, γ_2, γ_3] = [4.5, 1.94, 0.502, 2.25, 0.97, 2.01] 10^{13}rad/s; (L = 400nm) [λ_1, λ_2, λ_3] = [463.8, 484.6, 491] nm, [κ_1, κ_2, κ_3, γ_1, γ_2, γ_3] = [4.06, 3.89, 0.426, 2.03, 1.95, 1.92] 10^{13}rad/s; (L = 420nm) [λ_1, λ_2, λ_3] = [461.6, 491.9, 504.3] nm, [κ_1, κ_2, κ_3, γ_1, γ_2, γ_3] = [4.08, 0.851, 1.49, 2.04, 1.92, 0.934] 10^{13}rad/s; (L = 440nm) [λ_1, λ_2, λ_3] = [461.9, 491.6, 521.3] nm, [κ_1, κ_2, κ_3, γ_1, γ_2, γ_3] = [4.08, 1.92, 1.45, 2.73, 1.92, 3.61] 10^{13}rad/s.

#217583 - $15.00 USD Received 22 Jul 2014; revised 17 Sep 2014; accepted 29 Sep 2014; published 8 Oct 2014

4. Conclusion

In summary, we have numerically and analytically demonstrated the PIT effect in a MDM bus waveguide coupled to a single multimode stub resonator. By manipulating the length or width of the stub resonator, we can obtain PIT windows in the plasmonic stub waveguide, and hence achieve the desired slow light effect. Moreover, the EIT-like spectral responses obtained theoretically are in good agreement with the rigorous FDTD simulations, which reveals that the PIT is attributed to the destructive interference between the resonance modes in the plasmonic stub resonator. In particular, the plasmonic system exhibits double transparency windows when adjusting L from 360nm to 440nm, and the double PIT response has only been shown in three-resonator system [8], highlighting our idea for the realization of double PIT windows in a single stub resonator. Owning to the simple configuration and compactness, the ultracompact structure holds great potential in sensitive sensor, optical switching and optical data storage in highly integrated optical circuits.

Acknowledgments

The authors are grateful to Prof. Yunfeng Xiao, Beibei Li and Yin Huang for their helpful discussions. This work was funded by the Fundamental Research Funds for the Central Universities of Central South University under Grant No. 2012zzts007 and 2013zzts009, the Research Fund for the Doctoral Program of Higher Education of China under Grant No. 20100162110068 and the National Natural Science Foundation of China under Grant No. 61275174.

#217583 - $15.00 USD Received 22 Jul 2014; revised 17 Sep 2014; accepted 29 Sep 2014; published 8 Oct 2014